3.1.5. SPECIAL STUDIES

Comparison of Aerosol Light Scattering and Absorption Measurements at Mauna Loa, Hawaii

CMDL has measured both aerosol light scattering (since 1974) and aerosol light absorption (since 1990) at MLO. In spring 2000 new light scattering and absorption instruments were installed at Mauna Loa (within 2 m of the old instruments). Prior to the upgrade, light scattering was measured with a three-wavelength nephelometer (MS Electron, Seattle, Washington), and light absorption was measured with an aethalometer (Magee Scientific, Berkeley, California). This original sampling system did not include size or relative humidity control of the aerosol sample. The new instruments are designated MLN (Mauna Loa New) to distinguish them from the collocated MLO instruments. The new system obtains measurements at two size cuts by using a valve to switch between a 10-μm and 1-μm impactor. Relative humidity is maintained at no more than 40% by heating the air sample as necessary. Table 3.5 lists the instruments and their period of operation at Mauna Loa.

It is important to assess how measurements from these instruments compare in order to maintain data consistency for the entire measurement period. The MLO and MLN systems were operated simultaneously for approximately 1 year (spring 2000–spring 2001). One year of simultaneous light scattering and 3 months of light absorption (the aethalometer broke in August 2000) measurements from the collocated instruments are compared here.

The comparison procedure was as follows:

- Select data for the overlap period, May 2000 through April 2001.
- Estimate the absorption coefficient for the aethalometer using $\sigma_{ap} = 10\ m^2\ g^{-1} \times [BC]$.
- Apply quality-control edit corrections to data sets (e.g., remove spikes and contaminated data).
- For the MLN data set, use only 10-μm size cut data.
- Correct the MLN PSAP data for (a) scattering by particles within the filter and (b) spot size. Also, remove low transmittance data (e.g., transmittance <0.5, per *Bond et al.* [1999]).
- Calculate hourly averages of scattering and absorption coefficients.
- Determine the least-squares linear fit and correlation coefficient for the data sets. Perform the regression for both a calculated and forced-to-zero *y*-intercept.

Figure 3.5 shows that, on an hourly basis, there is excellent correlation between the nephelometer measurements ($R^2 = 0.94$), and the instruments agree fairly well (the slope is 1.1). This agreement is also seen when the data are separated for upslope (polluted) and downslope (cleaner) conditions. Because the two instruments appear to be in good agreement, the old nephelometer was removed during annual maintenance in May 2001.

The comparison between the PSAP and the aethalometer (Figure 3.6) was over a much shorter time period: May 2000-early August 2000. In early August the aethalometer feed sprocket was replaced, and after the replacement, measurements from the two instruments became completely uncorrelated ($R^2 = 0.02$). Prior to the feed sprocket replacement, the absorption measurements show that the PSAP measured absorption coefficients ~3 times higher than the aethalometer although the instruments were fairly well correlated ($R^2 \approx 0.6$). The difference between the two instruments suggests that the assumed BC absorption efficiency of 10 $m^2\ g^{-1}$ may not be appropriate for Mauna Loa. Additional comparisons between the PSAP and aethalometer are planned to resolve this discrepancy.

TABLE 3.5. Instrument Inventory at Mauna Loa Observatory

Instrument	Period of Operation	Station	Comments
MRI nephelometer	1974-spring 2000	MLO	Four wavelengths, no size cut
MRI nephelometer (operating at one wavelength because of instrument problems)	Summer 1982-spring 1984	MLO	One wavelength (550 nm), no size cut
MS Electron nephelometer	Spring 1994-spring 2001	MLO	Three wavelengths, no size cut
Magee Scientific aethalometer	1990-present	MLO	Broadband, no size cut; specific absorption of 10 $m^2\ g^{-1}$ used to convert [BC] to σ_{ap}
TSI nephelometer (model number 3563)	Spring 2000-present	MLN	Three wavelengths, total and back scatter, 1- and 10-μm size cuts
Radiance Research particle soot absorption photometer (PSAP)	Spring 2000-present	MLN	565-nm wavelength, 1- and 10-μm size cuts

MRI, Meteorology Research Inc.

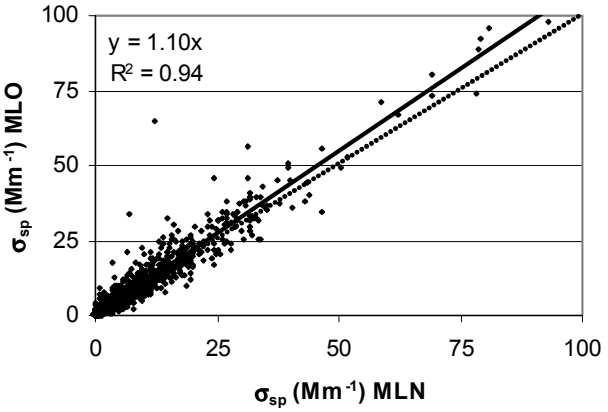

Fig. 3.5. Comparison of scattering measured by the new nephelometer (σ_{sp} MLN) with scattering measured by the old nephelometer (σ_{sp} MLO) for 550-nm wavelength, spring 2000-spring 2001. The solid black line shows the fit when the *y*-intercept is forced through the origin; the dashed line is the 1:1 line.

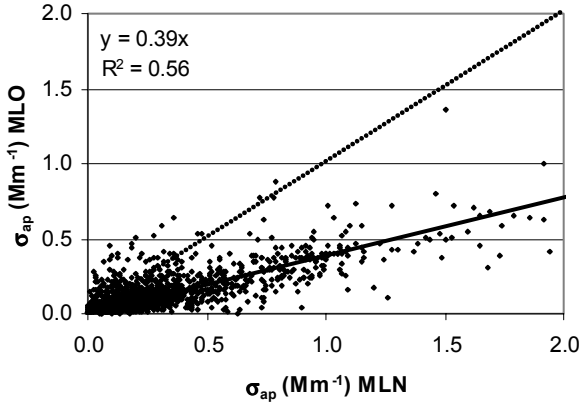

Fig. 3.6. Comparison of absorption measured by the PSAP (σ_{ap} MLN) with absorption measured by the aethalometer (σ_{ap} MLO), May 2000-August 2000. The solid black line shows the fit when the *y*-intercept is forced through the origin; the dashed line is the 1:1 line.

Determination of the Light Absorption Efficiency of Graphitic Carbon in Indian Ocean Aerosols

Carbonaceous particles in the atmosphere are generally thought to contain up to two major classes of carbon: organic carbon (OC) and black carbon (BC, also called elemental carbon, EC). Visible light absorption by atmospheric aerosols is typically dominated by particles containing BC. The mass measurement of BC in atmospheric aerosol samples has most often been performed by thermal evolved gas analysis [e.g., *Cachier et al.*, 1989] or thermal optical reflectance (TOR) methods [e.g., *Chow et al.*, 1993]. The light absorption coefficient (σ_{ap}) of aerosol samples has been determined with optical (usually filter-based) instruments, such as the aethalometer [e.g., *Bodhaine*, 1995], the PSAP [e.g., *Bond et al.*, 1999], or photoacoustic techniques [e.g., *Arnott et al.*, 1999]. All of these measurement techniques depend directly on the amount of aerosol sampled for the analysis, and all have associated measurement uncertainties, artifacts, interferences, and other problems that must be taken into account.

A measure of the efficiency with which atmospheric aerosols absorb visible radiation is desirable for model inputs and other applications. The aerosol light absorption efficiency, α, is defined as

$$\alpha = \sigma_{ap}/m_c \,, \qquad (1)$$

where σ_{ap} is total absorption (in Mm^{-1}), and m_c is the mass concentration of absorbing carbon (in $\mu g\ m^{-3}$). The parameter α has also been called the specific attenuation cross section, the specific absorption coefficient, and the BC mass absorption coefficient in previous studies. Over the past two decades, reported values of α have ranged from ~1 to 25 $m^2\ g^{-1}$. Most of the variability in α has been attributed to differences in aerosol composition, shape, size, mixing state (i.e., internal vs. external), and amount of scattering material present. The challenge for researchers is to determine what portion of the variability in α is caused by instrument uncertainty or differences in measurement methods and what portion is due to real differences in the studied aerosols.

A new method of determining the α of graphitic carbon (GC), a specific and dominant component of BC, is reported here. The PSAP instrument was used to obtain the σ_{ap} of aerosol samples collected during the Indian Ocean Experiment (INDOEX) in early 1999. The PSAP is a filter-based instrument in which aerosol particles are continuously deposited onto a filter. A transmittance measurement is made through the particle deposit and simultaneously compared with an identical measurement through a second, particle-free filter. Through careful calibration of the raw transmittance signals against derived absorption from an extinction cell/nephelometer system [*Bond et al.*, 1999], a measurement of suspended-state aerosol absorption is obtained.

For the analysis of GC mass, CMDL collaborated with colleagues at the Institute for Tropospheric Research (IFT) in Leipzig, Germany. The Raman instrument used in this study to quantify GC mass was a Bruker IFS 55 spectrometer equipped with a FRA-106 Raman module in a backscatter configuration. Calibration of the Raman spectrometer for GC mass on the PSAP filters was performed as documented in *Mertes et al.* [2002] using a commercially available carbon black standard (Monarch 71, Cabot Corporation, Boston, Massachusetts). The atmospheric concentration of GC can then be calculated from the GC filter mass, using the volume of air sampled through the PSAP filters.

This investigation has two advantages over previous studies. First, the GC responsible for light absorption and

not the thermographic EC is used. Thus, a quantifiable, dominant component of light absorbing carbon is obtained. Second, the correlation between σ_{ap} and m_c is analyzed from identical aerosol samples (i.e., the same particles), so any variability between samples does not come from examining different populations of particles in the two analyses.

The INDOEX Intensive Field Phase (IFP) was conducted during February and March 1999. The site for CMDL surface measurements was the Kaashidhoo Climate Observatory (KCO), on the island of Kaashidhoo in the Republic of Maldives. During this period of the winter monsoon, dry winds from the northeast sweep over the area. These winds bring very polluted air from India and Southeast Asia over the Maldives. The INDOEX aerosols have been found to contain significant fractions of BC [*Ramanathan et al.*, 2001]; probable sources of these aerosols include biomass and biofuel burning, vehicle exhaust, industrial releases, and other anthropogenic emissions.

Figure 3.7 shows a time series of σ_{ap} plotted alongside GC concentration. Overall, there was good agreement between the two parameters over the course of the IFP. The initial portion of the experiment (through DOY 70) was a period of higher aerosol concentrations at KCO punctuated by two rainfall events that removed aerosols from the atmosphere. From DOY 71 through nearly the end of the IFP, light absorption coefficients were relatively lower, but still several times larger than at typical rural, midcontinental sites in the United States [*Delene and Ogren*, 2002]. In Figure 3.7, each symbol represents the analysis of one PSAP filter. When high concentrations of aerosols were present, filters were changed up to five times per day to prevent the PSAP filter transmittance measurement from dropping below 0.5. During cleaner periods (e.g., the rainfall events), filters were changed as infrequently as once per day.

Figure 3.8 shows σ_{ap} plotted against GC. In this analysis, the PSAP filters were grouped according to their filter loading, and one obvious outlier was removed from the "Medium Loading" category. The PSAP manufacturer's manual states that absorption measurements should be reliable as long as the filter transmittance (Tr, or I/I_0) remains above 0.5. The calibrations recommended by *Bond et al.* [1999], however, were performed using PSAPs with Tr values maintained above 0.7, so this grouping of lightly loaded filters is the only one in which the *Bond et al.* [1999] PSAP calibration corrections can be applied reliably. The slope of the linear least squares regression line through the lightly loaded filters equates to an α of 9.7 m^2 g^{-1}, with a very small offset and an R^2 value of 0.86. The filters with higher GC loadings show regression slopes between roughly 9.0 and 10.4, but with significant y-intercepts. These zero offsets may be due to uncertainties in the nonlinear filter loading corrections used in the PSAP instrument. While GC currently is thought to be the major aerosol absorber of visible radiation, other forms of carbonaceous material (e.g., amorphous C, organic C) need to be studied in a similar manner to quantify their contributions to visible light absorption by aerosols.

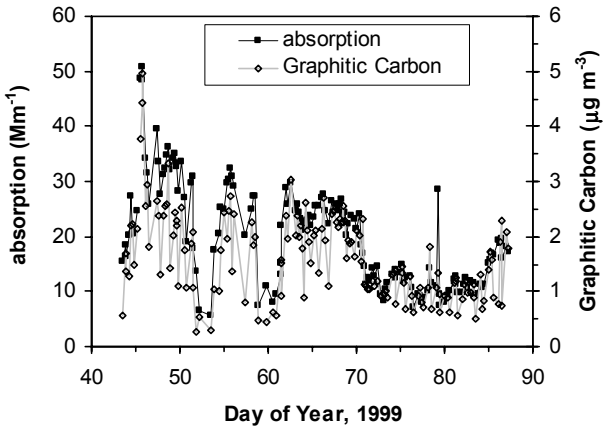

Fig. 3.7. Time series of absorption and graphitic carbon measured at KCO during February-March 1999.

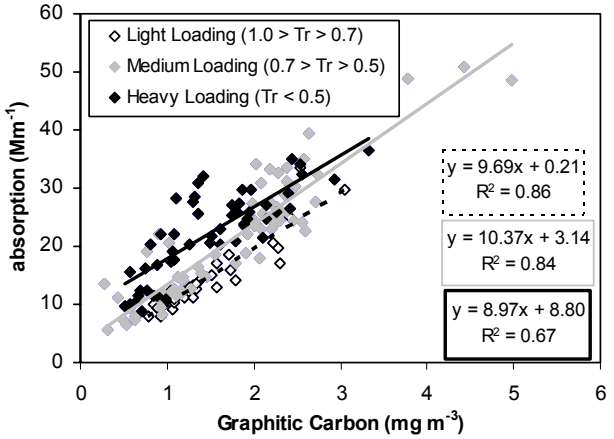

Fig. 3.8. Comparison of GC and absorption coefficient measured at KCO during February-March 1999. The solid dark line is the fit to the heavy loading data; the gray line is the fit to the medium loading data; and the dashed black line is the fit to the light loading data. One outlier has been removed from the "Medium Loading" data set.

In Situ Aerosol Profile Measurements over the Southern Great Plains Cloud and Radiation Testbed (CART) Site

The objective of this project is to obtain a statistically significant data set of in situ measurements of the vertical distribution of aerosol properties (e.g., light scattering and absorption). The measurements will be used to answer the following scientific questions:

- How do aerosol properties vary throughout the year?
- Under what conditions can surface-based measurements of these properties be used to calculate the direct aerosol radiative forcing from a measured aerosol optical depth (and what conditions inhibit such calculations)?
- How do local and regional perturbations (e.g., fires) influence the vertical profile characteristics?
- How do data from these flights compare with other measurements of atmospheric characteristics, e.g., aerosol optical depth (AOD)?

The data are obtained on an instrumented light aircraft (Cessna C-172N) over the Southern Great Plains (SGP) CART site in Lamont, Oklahoma. The aerosol instrument package on the aircraft is similar to the one operating at the surface SGP site. The aircraft flew 225 profile flights between March 2000 and December 2001. For each profile flight, the Cessna flew nine level legs over (or near) the SGP site. The legs were flown at altitudes of 467, 610, 915, 1220, 1525, 1830, 2440, 3050, and 3660 m above sea level, and flights were made several times each week. Aerosol data were collected at 1 Hz and averaged over the duration of each level flight segment (~10-min averages for the four highest levels, ~5-min averages for the five lowest levels). Aerosol optical properties obtained for each level leg include σ_{sp}, σ_{bsp}, and σ_{ap} coefficients. From these extensive properties the following intensive aerosol optical properties were derived: ω_o, b, and $\mathring{a}$. All measurements on the aircraft were made at low humidity (RH $\leq$ 40%).

There is good agreement ($R^2 = 0.82$) between lowest level leg and surface extinction ($\sigma_{ext} = \sigma_{ap} + \sigma_{sp}$) values, indicating submicrometer aerosol (predominantly scattering aerosol) in the 150 m above the surface is well-mixed. Much of the variability in the parameters measured at the surface site appears to be captured by the weekly profiling flights. The comparison is not as good ($R^2 = 0.49$) for single-scattering albedo and is due to measured differences in absorption between the surface and the lowest flight level. These observed differences appear to be real because side-by-side tests of the two PSAPs show good agreement (within 8%). Comparison of other derived properties at the lowest flight level with surface properties are excellent for backscatter fraction and green-blue Ångström exponent, but less so for the green-red Ångström exponent.

Figure 3.9 shows the medians and ranges (as indicated by percentiles) of a representative extensive aerosol optical property (extinction) and a representative intensive aerosol optical property (single-scattering albedo) at STP, low RH, and $D < 1$ μm, obtained at the surface and during vertical profiling flights. The line in the center of the box represents the median, while the edges of the box give the 25th and 75th percentiles, and the whiskers extend to the 5th, and 95th percentiles. In general, the values for extensive properties (extinction, absorption, and scattering coefficients) vary by up to a factor of 3, while the medians for intensive aerosol properties (single scattering albedo, backscatter fraction, and Ångström exponent) are much less variable (less than 10% variation). Figure 3.9 suggests that the median values of the extensive properties tend to decrease with altitude from the surface upward. Such behavior is expected as distance from the ground-based sources of aerosol particles increases. The median values of the intensive properties do not display a strong dependence with altitude.

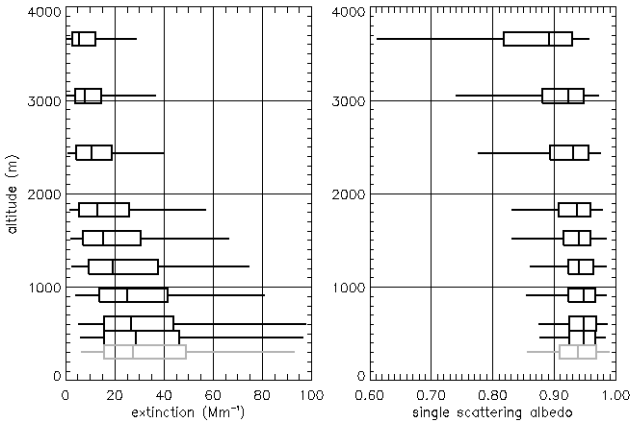

Fig. 3.9. Statistical box and whisker plots of vertical profiles of extinction (left) and albedo (right) over the SGP site, March 2000-March 2001. Black plots are from aircraft flights; gray plots are surface measurements. The boxes and whiskers are as in Figure 3.1.

More indicative of the overall variability of the aerosol are the ranges of the parameters, as indicated by the percentiles in Figure 3.9. Extensive properties can differ by up to 2 orders of magnitude between flights and even between individual levels of the same flight. The intensive properties, while still displaying a range of values, vary at most by an order of magnitude (i.e., green-red Ångström exponent, level 3660 m) but more commonly by less than a factor of 2. The parameter ranges display different tendencies with height. Extensive properties become less variable at higher altitudes, due to consistently low concentrations of aerosol particles. Conversely, intensive properties become more variable with altitude for a similar reason: low concentrations of aerosol particles result in more noise when calculating the values of these parameters.

The surface measurements are representative of the frequency distributions aloft, particularly for intensive properties such as albedo (Figure 3.9). However, the correlations (not shown) between column average and surface values are lower (e.g., extinction $R^2 = 0.65$; albedo $R^2 = 0.30$) than correlations between lowest flight level and surface values. Thus, while surface aerosol measurements are statistically representative of the air aloft, they may not be representative of day-to-day variations in the column.

Measurements from the profile flights can also be compared with measurements by remote sensing instruments located at SGP, i.e., the Cimel sun/sky radiometer and the multi-filter rotating shadowband radiometer (MFRSR). After incorporation of corrections for supermicrometer, upper tropospheric, and stratospheric aerosol particles, comparison in Figure 3.10 of aerosol optical depth (AOD) calculated from aircraft measurements with AOD obtained from the remote sensing instruments shows fair correlation ($R^2 \approx 0.5$, Cimel; $R^2 \approx 0.8$, MFRSR), although the aircraft AODs are lower than those derived from the radiation instruments, with an offset in the range of –0.03 or –0.04.

Long-term surface measurements can represent a statistical distribution of aerosol properties aloft. However, day-to-day variability between the surface and aloft may not always be captured and causes a poor relationship between surface and column average quantities. Comparison of the in situ and remote sensing instruments shows fair correlation for AOD although the aircraft AOD is consistently lower than that of the remote sensing instruments.

Measurements of Aerosol Optical Properties from a Surface Site in Korea (ACE-Asia)

An intensive field campaign known as the Asian Pacific Regional Aerosol Characterization Experiment (ACE-Asia) took place in April 2001 in eastern Asia. The goal of ACE-Asia was to gather data for regional climate models as well as to understand better the interactions between aerosols and radiation, gas phase species, transport, and clouds.

This large field study was a multi-platform, international effort with scientific measurements being recorded from land-based sites, ships, aircraft, and satellites. Scientists from Korea, United States, Great Britain, China, Japan, and Australia worked together to characterize aerosol radiative, chemical, and size properties. These aerosol properties, as well as their covariance, strongly influence the Earth's radiative balance. The primary surface site was located at the Upper Air Meteorological Observation Facility near the small town of Kosan on Cheju Island, South Korea. The site is strategically located between several major aerosol source regions. Depending on wind conditions, the scientists observed anthropogenic aerosol from Japan, Korea, and China; large dust outbreaks from northern China; relatively clean marine air; or even local crop burning.

As part of this effort, CMDL conducted in situ measurements of the aerosol optical properties as well as full column measurements of solar radiation at Kosan. The ground-based measurements included aerosol scattering coefficient as a function of particle size, wavelength, and relative humidity, and the aerosol absorption coefficient as a function of size. These observations provide a direct measure of the surface aerosol extinction of visible radiation. For full column measurements of the atmosphere, radiometers from CMDL measured the total, direct, and diffuse (scattered light by aerosol) solar radiation. These observations can be used to derive the AOD, or amount of solar radiation attenuated by aerosols, and the aerosol forcing efficiency.

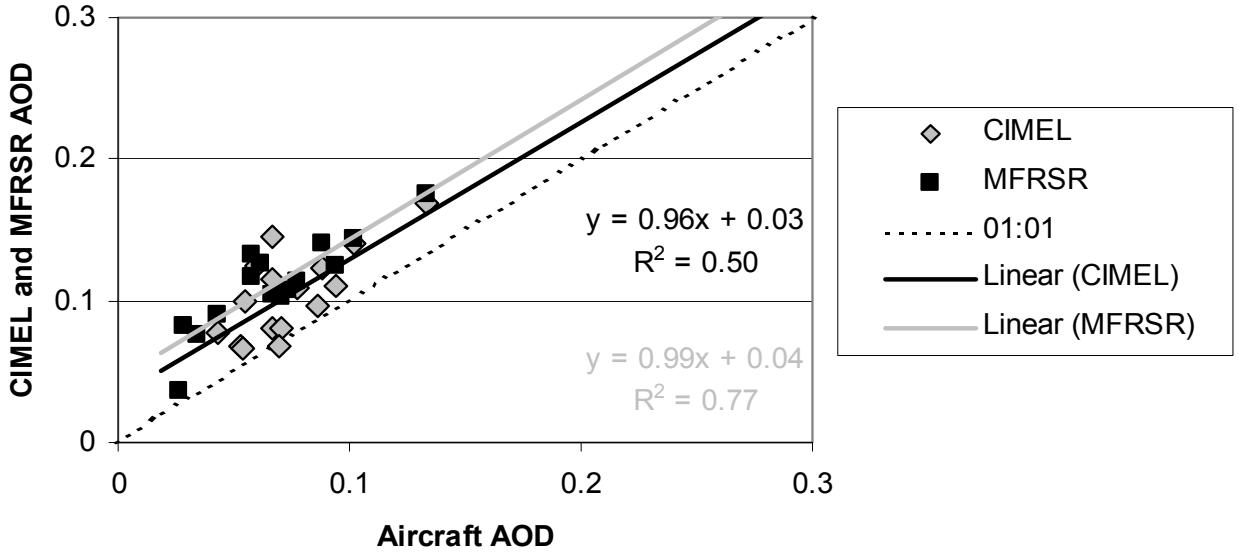

Fig. 3.10. Comparison of aerosol optical depth (AOD) measured on aircraft with AOD derived from Cimel and MFRSR remote sensing instruments at the SGP site, for March 2000-March 2001.

The aerosol scattering coefficient was highly variable during the campaign, ranging between 20 and 250 Mm^{-1}. Spring in Korea is known as the dust season when southeasterly winds bring dust to the region from the Gobi Desert. Several such events, note particularly day of year (DOY) 101-104 and DOY 110, are apparent from the data (Figure 3.11). On these days over 60% of the aerosol scattering was in the total size mode, as indicated by the low values of the ratio of the submicrometer to total aerosol scattering coefficients (Figure 3.11c). The aerosol single-scattering albedo during the dust events declined slightly to ~0.80 for total aerosol and as low as 0.63 for submicrometer aerosol (Figure 3.11b). Most of the aerosol absorption during the campaign was in the submicrometer particles. The aerosol hygroscopic growth factor, $f(RH) = \sigma_{sp}(RH=85)/\sigma_{sp}(RH=40)$, a measure of the increase in scattering due to aerosol water uptake, was relatively high during the dust events, ranging from 1.5 to 2.5 (Figure 3.11d). The low single-scattering albedo and high hygroscopic growth factor indicate the aerosol at the site was composed of not only dust but also very likely of absorbing elemental and hygroscopic species such as sulfate, oxidized organics, and seasalt.

Mean aerosol optical properties from Kosan as well as from two other anthropogenically perturbed sites are given in Table 3.6. Although all three sites receive anthropogenic aerosol, there are significant differences in the aerosol optical properties between the sites, demonstrating the importance of long-term, regional measurements at a variety of locations. Kosan, South Korea, and Kaashidhoo, Republic of Maldives, are anthropogenically perturbed marine sites, and Bondville, Illinois, is an anthropogenically perturbed continental site. The aerosol scattering coefficient from Kosan is higher than from either the Kaashidhoo or the Bondville site, indicating a high aerosol loading in eastern Asia during the spring. Kosan and Kaashidhoo have higher light absorption coefficients than Bondville, consistent with a larger contribution of combustion aerosol (e.g., from biomass burning or limited pollution control on vehicles and industries). Consistent with the higher absorption coefficients at Kosan and Kaashidhoo, those sites have lower single-scattering albedo values than Bondville, with Kaashidhoo being significantly lower than Kosan. The $f(RH)$ value at Kosan was significantly higher than at Kaashidhoo or Bondville. The $f(RH)$ at Kosan did not correlate well with seasalt aerosol,

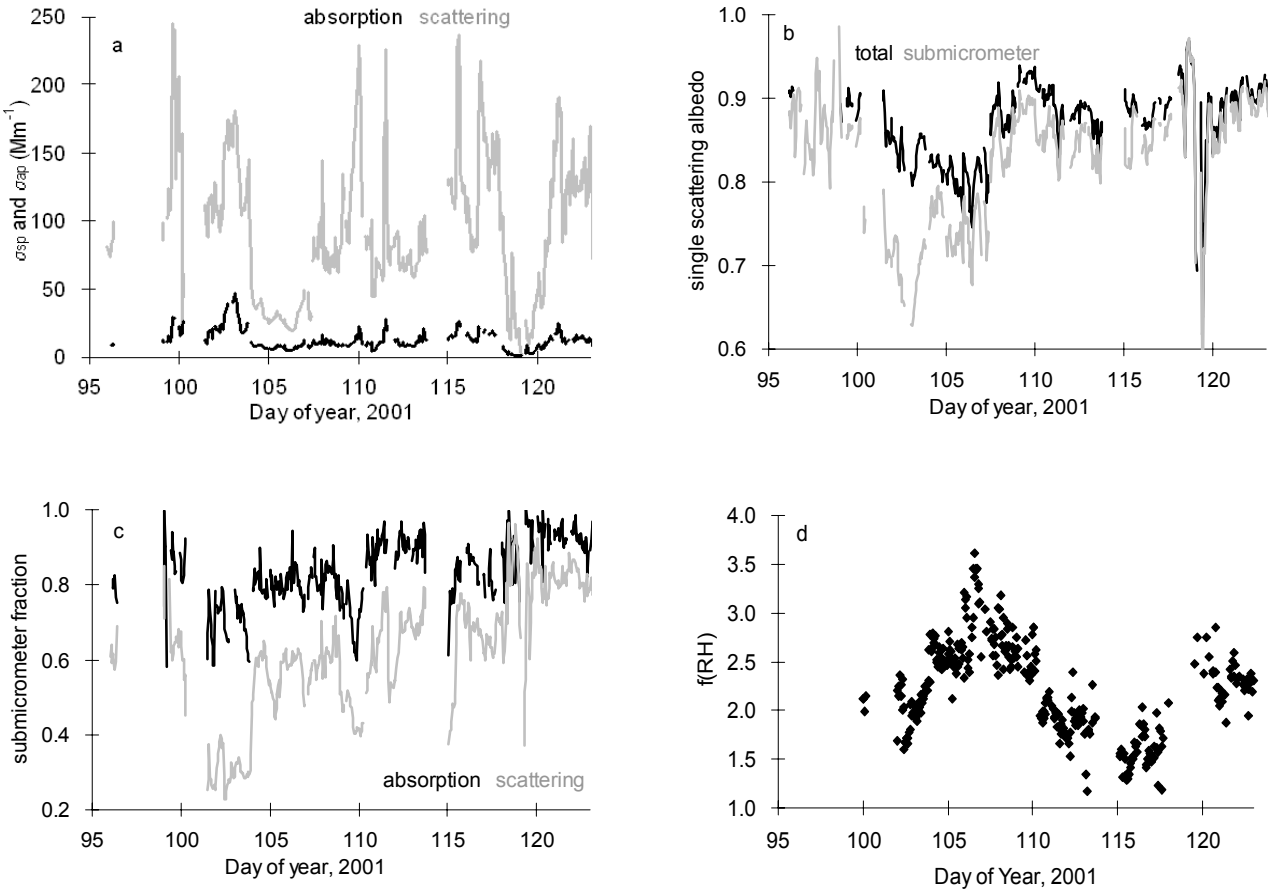

Fig. 3.11. Time series of aerosol measurements from Kosan during ACE-Asia in 2001: (a) total absorption and scattering coefficients, (b) total and submicrometer single-scattering albedo, (c) submicrometer fraction of aerosol absorption and scattering, and (d) total aerosol hygroscopic growth factor. All values are reported for a wavelength of 550 nm.

TABLE 3.6. Means and Standard Deviations of Aerosol Optical Properties of Anthropogenically Influenced Aerosols at 550 nm

Aerosol Property	Kosan (KOS)	Kaashidhoo (KCO)	Bondville (BND)
σ_{sp}*	92 (53)	73 (28)	54 (43)
σ_{ap}*	12 (8)	16 (9)	4 (3)
ω_o	0.87 (0.05)	0.82 (0.03)	0.92 (0.06)
f(RH)	2.2 (0.5)	1.7 (0.1)	1.7 (0.4)†
$F\sigma_{sp}$‡	0.61 (0.16)	0.67 (0.08)	0.86 (0.09)
$F\sigma_{ap}$‡	0.83 (0.09)	0.84 (0.06)	0.92 (0.38)

KOS data for April 2001; KCO data for mid-February-March 1999; BND data for all of 2000.

*Values are for total (D < 10 μm) aerosol.

†*Rood,* personal communication, 2002.

‡$F\sigma_{sp}$ and $F\sigma_{ap}$ are the submicrometer fractions of aerosol scattering and absorption, respectively.

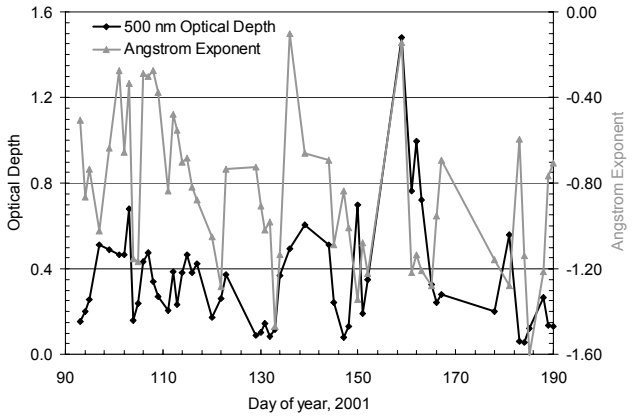

Fig. 3.12. Aerosol optical depth measured at 500 nm and aerosol Ångström exponent from the 412/862-nm wavelength pair, March 31-July 9, 2001, at Kosan.

but was probably high due to extensive mixing with polluted air masses containing sulfates and nitrates from both China and Korea as well as cloud processing. At Kaashidhoo the aerosol was more reflective of the source emissions, which were high in black carbon and, periodically, dust and had undergone little cloud processing. The strong inversion layer present during the INDOEX sampling at Kaashidhoo prevented significant processing of the aerosol in the boundary layer, whereas the frontal systems present during ACE-Asia promoted strong vertical mixing between the boundary layer and lower free troposphere and hence faster aerosol cloud processing. The similarity of the f(RH) values at KCO and BND is most likely coincidental and not from a similar aerosol composition. Finally, at all three sites, the absorbing aerosol was concentrated in the submicrometer aerosol, as suggested by the high values of the submicrometer fraction of absorbing aerosol (Table 3.6). However, Kosan and Kaashidhoo had lower values of the submicrometer fraction of scattering aerosol than Bondville, most likely due to the presence of seasalt and/or dust at those two sites.

The sunphotometers give a measure of the direct solar irradiance in seven narrowband wavelength channels. Preliminary data from these instruments (screened for clouds) give a measure of the AOD. On days with the highest pollution, the AOD for 500-nm radiation was as high as 0.7, and on days with clean marine air the value dropped to a low of 0.1. During the major dust event from DOY 101 to 104 the AOD was 0.45 to 0.7, indicating relatively low sunlight levels from a heavy loading of aerosol. **Figure 3.12** shows both the AOD at 500 nm and the aerosol Ångström exponent, a measure of the aerosol size, for a 3-mo period from March 31 to July 9, 2001, at Kosan.

Systematic Variation of Aerosol Optical Properties

Aerosol optical properties measured over several years at BND, SGP, WSA, and BRW have been analyzed to determine the importance of the variability in aerosol optical properties to direct aerosol radiative forcing calculations and to investigate whether systematic relationships exist between various aerosol optical properties, i.e., σ_{ap}, ω_o, b, $å$, and aerosol radiative forcing ($\Delta F/\delta$), and the amount of aerosol present (measured as σ_{sp}). Systematic relationships among aerosol properties can be used to check for consistency among measured and modeled climatologies. Also, systematic relationships can be used in model parameterization to reduce uncertainties resulting from insufficient knowledge of aerosol properties. The performance of different models can be evaluated with measurements, and if models predict the parameters that are observed, the measurements can be used to validate the models.

Knowledge concerning systematic relationships among aerosol properties can be useful in reducing uncertainties in remotely sensed data because they can be used to make better assumptions about unknown aerosol properties. *Remer and Kaufman* [1998] illustrated the importance of using a dynamic model where aerosol properties vary with aerosol load for the inversion of remote sensing data. The reason to use a dynamic aerosol model is to represent systematic changes in one aerosol property as another property changes. Because of their importance and usefulness, systematic relationships among aerosol optical properties were investigated at the four surface sites. Figure 3.13 shows systematic relationships among low relative humidity (<40%), aerosol optical properties (σ_{ap}, ω_o, b, and $\Delta F/\delta$), and the aerosol load (measured as σ_{sp} at 550-nm wavelength). The mean aerosol optical properties were calculated over σ_{sp} intervals of 10 Mm^{-1}, and the corresponding maximum standard error for each station is given in the graph. The standard errors are considerably smaller than the changes over 10-Mm^{-1} bins, which implies a high level of significance to the relationships. The σ_{ap} does not increase as rapidly as the σ_{sp}, resulting in a systematic increase in ω_o as σ_{sp} increases at all four stations. All four stations also show a systematic decrease

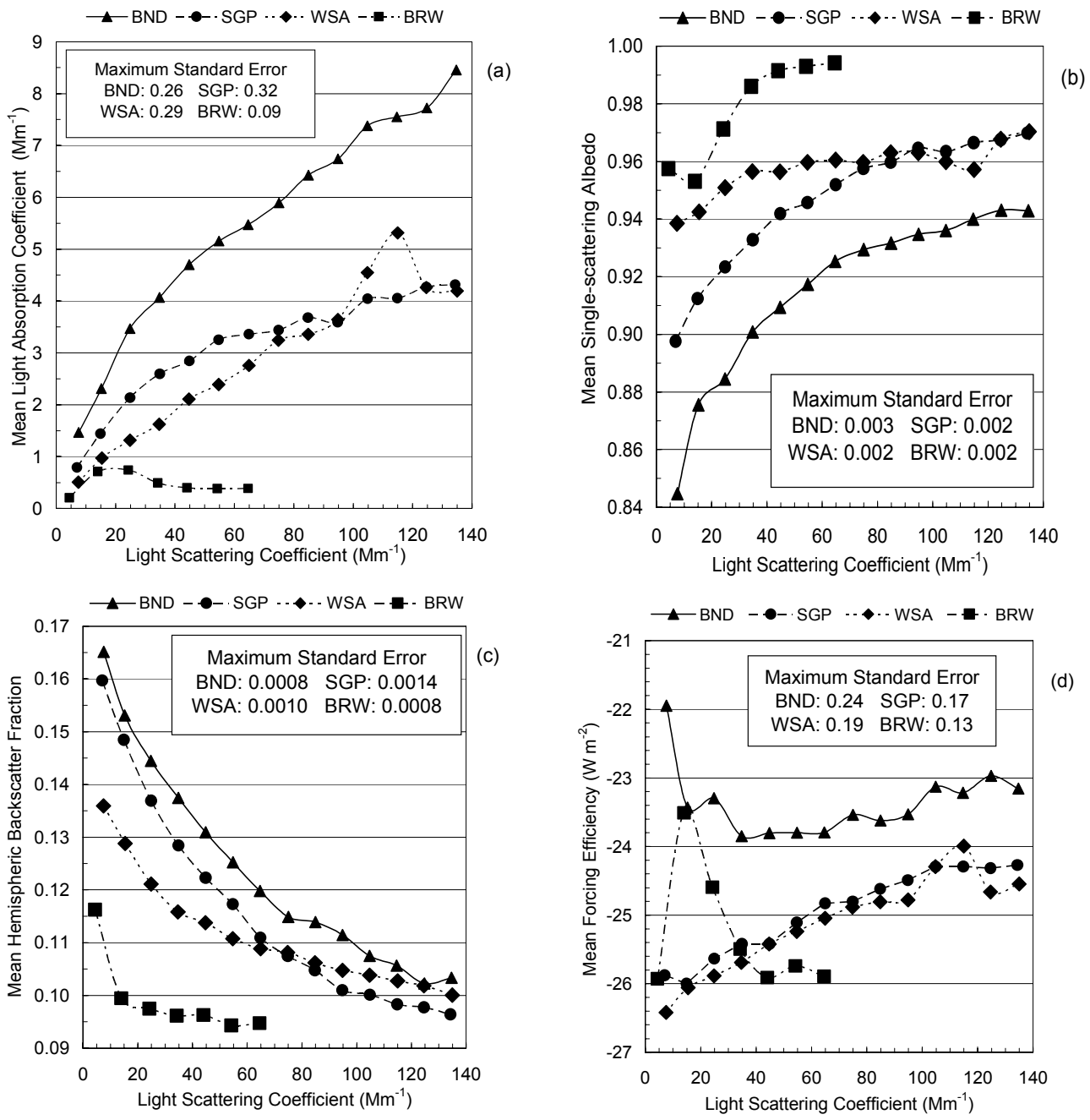

Fig. 3.13. (a) Mean aerosol light absorption coefficient (σ_{ap}), (b) mean single-scattering albedo (ω_0), (c) mean hemispheric backscatter fraction (b), and (d) mean forcing efficiency ($\Delta F/\delta$), all versus the aerosol light scattering coefficient (σ_{sp}), for BND, SGP, WSA, and BRW. Plots are based on all valid hourly averaged aerosol measurements (>50% 1-min data within the hour) for systems with TSI 3563 nephelometers. The mean values were calculated over 10-Mm^{-1} σ_{sp} bins. The maximum standard error (sample standard deviation /square root of the number of points) at each station is given in the text boxes.

in b as σ_{sp} increases. In terms of $\Delta F/\delta$, the relationship between b and σ_{sp} acts to offset the relationship between ω_o and σ_{sp}. The b-σ_{sp} relationship results in a decrease in the magnitude of the $\Delta F/\delta$ as σ_{sp} increases, while the ω_o-σ_{sp} relationship results in an increase in the magnitude of the $\Delta F/\delta$ as σ_{sp} increases. For SGP and WSA, the b-σ_{sp} relationship is more important and results in a decrease in the magnitude of $\Delta F/\delta$ as σ_{sp} increases. For BND, the ω_o-σ_{sp} relationship is more important for σ_{sp} less than 40 Mm^{-1} and results in an increase in the magnitude of $\Delta F/\delta$ as σ_{sp} increases; however above 40 Mm^{-1}, the b-σ_{sp} relationship is more important and results in a decrease in the magnitude of $\Delta F/\delta$ as σ_{sp} increases. Similarly at BRW, the relative importance of one relationship compared with the other determines how $\Delta F/\delta$ changes as σ_{sp} increases.

Figure 3.14 illustrates two systematic relationships, one between $å$ and σ_{sp} and the other between submicrometer scattering fraction R_{sp} and $å$. The strong relationship between R_{sp} and $å$ indicates that $å$ is sensitive to changes in the relative amount of submicrometer scattering aerosol. At BND and SGP $å$ decreases as σ_{sp} drops below 30 Mm^{-1}, whereas at WSA and BRW $å$ increases as σ_{sp} drops below 30 Mm^{-1} (Figure 3.14a). Above 30 Mm^{-1} all four stations show a fairly constant $å$ with increasing σ_{sp}. This systematic relationship suggests that during low aerosol concentration events, the continental sites (BND and SGP) have more relatively larger particles present, while the marine sites (WSA and BRW) have more relatively smaller particles present. The $å$-σ_{sp} relationship at BND and SGP is consistent with the relationship between the Ångström exponent and aerosol optical thickness (derived from Sun/sky scanning spectral radiometer measurements) for the mid-Atlantic region of the eastern United States [*Remer and Kaufman*, 1998]. It is interesting to note that while the $å$-σ_{sp} relationship is different between SGP and WSA, the $\Delta F/\delta$-σ_{sp} relationship is very similar. This suggests that the $\Delta F/\delta$-σ_{sp} relationship is not influenced by changes in the submicrometer to total aerosol fraction but rather by changes in the submicrometer aerosol size distribution (b-σ_{sp} relationship) and the aerosol composition (ω_o-σ_{sp} relationship).

Systematic relationships exist between various aerosol properties (σ_{ap}, ω_o, b, $\Delta F/\delta$, and $å$) and σ_{sp} and also between $å$ and submicrometer scattering fraction R_{sp} (Figure 3.14b). These systematic relationships are qualitatively similar among the four stations; however, the quantitative relationships are different at each station, which is indicative of the occurrence of different aerosol types and size distributions at each station. Systematic relationships and the regional, yearly, weekly, and daily variations in optical properties can be used to check for consistency between climatologies based either on observations or models. The existence of systematic changes in aerosol optical properties with changes in aerosol concentration indicate that care should be taken when using average values in algorithms to retrieve aerosol properties, such as optical depth, from satellite data. An algorithm that uses a static representation for aerosol optical properties will have a systematic bias in derived values.

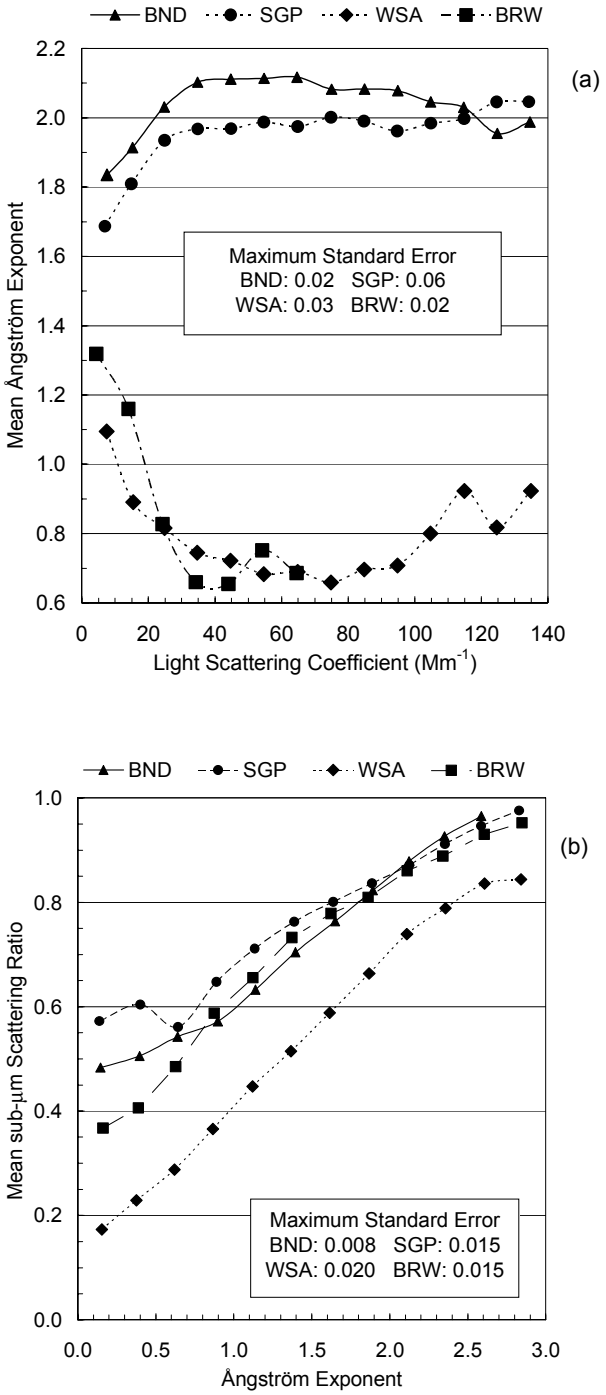

Fig. 3.14. (a) Mean Ångström exponent ($å$) versus aerosol light scattering coefficient (σ_{sp}) and (b) submicrometer scattering fraction (R_{sp}) versus Ångström exponent, for BND, SGP, WSA, and BRW. Plots are based on all valid hourly averaged aerosol measurements (>50% 1-min data within the hour) for systems with TSI 3563 nephelometers. The $å$ values were calculated over 10-Mm^{-1} σ_{sp} bins, and the mean R_{sp} was calculated from 0.25-Å exponent bins. The maximum standard error (sample standard deviation /square root of the number of points) at each station is given in the text boxes.